Available online at www.sciencedirect.com
SCIENCE DIRECT®
C. R. Mecanique 333 (2005) 726–731
COMPTES RENDUS MECANIQUE
http://france.elsevier.com/direct/CRAS2B/

Computational AeroAcoustics: from acoustic sources modeling to farfield radiated noise prediction

Computational aeroacoustics using the B-spline collocation method

Ronny Widjaja [a,*], Andrew Ooi [a], Li Chen [b], Richard Manasseh [c]

[a] *Department of Mechanical Engineering, University of Melbourne, Parkville, 3010, Australia*
[b] *Maritime Platforms Division, Defence Science Technology Organization, Fishermans Bend, 3027, Australia*
[c] *Energy and Thermofluids Engineering, Commonwealth Scientific and Industrial Research Organization, Highett, 3190, Australia*

Available online 8 September 2005

Abstract

One of the major problems in computational aero-acoustics is the disparity in length scales between the flow field and the acoustic field. As a result, a mapping function is normally used to achieve a non-uniform grid distribution. In this paper, a B-spline collocation method with an arbitrary grid placement capability is proposed. This capability not only allows an optimum grid distribution but also avoids the numerical complexities associated with the mapping function. The B-spline collocation method is applied to the case of spinning co-rotating vortices. The result agrees well with the matched asymptotic solution. ***To cite this article: R. Widjaja et al., C. R. Mecanique 333 (2005).***

Résumé

Collocation par B-spline appliquée aux simulations numériques en aéroacoustique. Un problème rencontré dans les simulations numériques en aéroacoustique est la disparité des échelles de longueur sur lesquelles sont résolus le champ de vitesse de l'écoulement fluide et le champ de pression acoustique. Habituellement une fonction de transformation est utilisée pour générer un maillage non-uniforme. Dans cet article une méthode de collocation par B-spline est proposée. Cette méthode permet un maillage optimum du domaine et évite les complexités numériques associées avec les fonctions de transformation. Le champ acoustique généré par une paire de tourbillons co-rotatifs est simulé en utilisant cette méthode. Les résultats de cette simulation numérique sont en accord avec la solution asymptotique associée. ***Pour citer cet article : R. Widjaja et al., C. R. Mecanique 333 (2005).***

Keywords: Acoustics; Computational aero-acoustics; B-spline collocation method

Mots-clés : Acoustique ; Simulation numérique en aéroacoustique ; Méthode de collocation par B-spline

* Corresponding author.
E-mail addresses: ronnyw@mame.mu.oz.au (R. Widjaja), a.ooi@unimelb.edu.au (A. Ooi), Li.Chen@dsto.defence.gov.au (L. Chen), Richard.Manasseh@csiro.au (R. Manasseh).

1631-0721/$ – see front matter
doi:10.1016/j.crme.2005.07.013

1. Introduction

Computational Aero-Acoustics (CAA) emerges from the success of Computational Fluid Dynamics (CFD) in solving many physical problems. Nevertheless, Tam [1] pointed out that there are some issues that are unique to CAA. These issues include the long-propagation distance and life of acoustic waves; and the disparity in length scales between the flow field and acoustic field. The former provides enough time for any dissipation and dispersion errors to grow and contaminate the acoustic field. The latter requires both a dense mesh and a large computational domain, causing a uniform mesh to be impractical in CAA.

To overcome the first issue, many studies have been conducted to improve the numerical schemes commonly used in CFD. Tam and Webb [2] developed a Dispersion-Relation-Preserving (DRP) scheme. This DRP scheme is an optimised finite difference scheme where the order of accuracy of the numerical scheme has been sacrificed for a much better resolution at high wave number. This considerably reduces the dispersion error. Another type of optimised scheme is the compact difference scheme with spectral-like resolution developed by Lele [3]. This scheme was further enhanced by Kim and Lee [4] using different optimisation constraints to ensure a minimum dispersion error over a certain range of wave number.

Unfortunately, all the above numerical schemes were developed by assuming uniform mesh. A mapping function is commonly used to extend the schemes for non-uniform mesh. The use of a mapping function usually results in more grid points than necessary and in some cases may lead to numerical instabilities. In this paper, an alternative approach using a B-spline collocation method is proposed. The B-spline collocation method is a collocation method using B-splines as the trial functions. Due to the flexibility of B-splines in the local representation, the B-spline collocation method allows the mesh points to be placed arbitrarily. This capability not only allows an optimum grid distribution but also avoids the numerical complexities associated with the use of a mapping function. Furthermore, a uniform C^{k-1} continuity throughout a B-spline element of order k gives the B-spline collocation method a high-resolution property.

2. Numerical formulations

The properties of the B-spline collocation method depend very much on the trial functions. A B-spline of order k is made up of a polynomial of order k and has a compact support consisting of $k+1$ knot points. Knot points are a set of points on which B-splines are defined. The distribution of these knot points determines the shape and distribution of the B-splines and consequently the resolution of the mesh.

Following the formulation by Morinishi, Tamano and Nakabayashi [5], the knot points $[t_{-k}, t_{-k+1}, \ldots, t_{N-1}, t_N]$ are related to the mesh points $[x_1, x_2, \ldots, x_{N-1}, x_N]$ by

$$t_j = \begin{cases} x_1 & \text{for } -k \leqslant j \leqslant 0 \\ \frac{1}{2}(x_{j+k/2} + x_{j+k/2+1} & \text{for } 0 < j < (N-k), \text{ even } k \\ x_{j+(k+1)/2} & \text{for } 0 < j < (N-k), \text{ odd } k \\ x_N & \text{for } (N-k) \leqslant j \leqslant N \end{cases}$$

The corresponding N numbers of B-splines of order k can be computed using the following recursive formula

$$B_j^k(x) = \frac{x - t_j}{t_{j+k} - t_j} B_j^{k-1}(x) + \frac{t_{j+k+1} - x}{t_{j+k+1} - t_{j+1}} B_{j+1}^{k-1}(x) \tag{1}$$

where the zeroth order B-spline is defined by

$$B_j^0(x) = \begin{cases} 1 & \text{for } t_j \leqslant x \leqslant t_{j+1} \\ 0 & \text{otherwise} \end{cases} \tag{2}$$

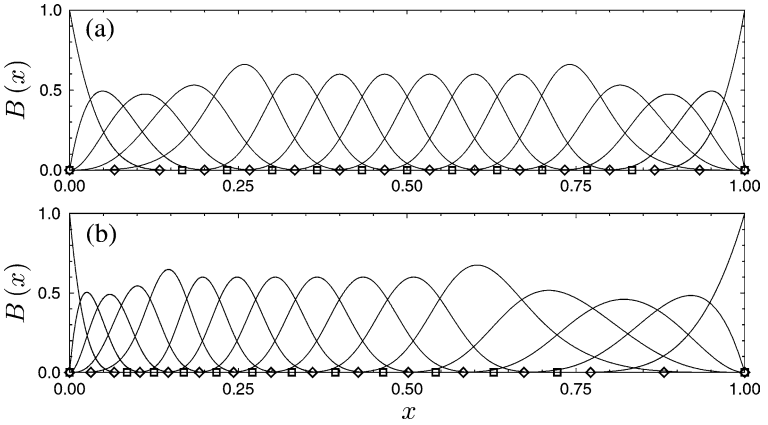

Fig. 1. Distributions of B-splines (——); knot points (□); and mesh points (◇) for (a) uniform mesh and (b) non-uniform mesh with local stretching factor of 0.1.

Fig. 1. Distribution des courbes B-splines (——) ; noeuds (□) ; et mailles (◇) du réseau pour (a) un maillage uniforme et (b) un maillage non uniforme avec un coefficient local d'étirement de 0.1.

The expressions for the first and second derivatives (i.e. $\frac{\mathrm{d}}{\mathrm{d}x}B_j^k(x)$ and $\frac{\mathrm{d}^2}{\mathrm{d}x^2}B_j^k(x)$) can be obtained by differentiating Eqs. (1) and (2) with respect to x.

To show a typical distribution of B-splines, consider a domain $x \in [0,1]$ discretized into 15 intervals with uniform and non-uniform grid spacings. The non-uniform mesh is constructed using a constant local stretching factor of $lsf = 0.1$ where the local stretching factor is defined as $lsf = \frac{x_{i+2}-x_{i+1}}{x_{i+1}-x_i} - 1$. The profiles of fourth order B-splines, $B_j^4(x)$, for both meshes are plotted in Fig. 1. Squares and diamonds represent the knot and mesh points respectively. The distribution of B-splines is clearly seen to follow the distribution of the knot points and the grid stretching is found to alter the shapes of the B-splines.

In solving differential equations, the computational variable (e.g. $\phi(x)$) and its derivatives are represented by a linear combination of B-spline trial functions as

$$\phi(x) = \sum_{j=1}^{N} \alpha_j B_j^k(x), \quad \frac{\mathrm{d}}{\mathrm{d}x}\phi(x) = \sum_{j=1}^{N} \alpha_j \frac{\mathrm{d}}{\mathrm{d}x} B_j^k(x), \quad \text{and} \quad \frac{\mathrm{d}^2}{\mathrm{d}x^2}\phi(x) = \sum_{j=1}^{N} \alpha_j \frac{\mathrm{d}^2}{\mathrm{d}x^2} B_j^k(x)$$

In matrix form, these equations can be written as

$$\{\phi\} = [M]\{\alpha\}, \quad \left\{\frac{\mathrm{d}\phi}{\mathrm{d}x}\right\} = [D]\{\alpha\} \quad \text{and} \quad \left\{\frac{\mathrm{d}^2\phi}{\mathrm{d}x^2}\right\} = [V]\{\alpha\}$$

where $M_{ij} = B_j^k(x_i)$, $D_{ij} = \frac{\mathrm{d}}{\mathrm{d}x}B_j^k(x_i)$ and $V_{ij} = \frac{\mathrm{d}^2}{\mathrm{d}x^2}B_j^k(x_i)$. These $[M]$, $[D]$ and $[V]$ matrices are in fact band-diagonal matrices where the elements of the matrices are non-zero only along the few diagonal lines adjacent to the main diagonal. As a result, conventional fast algorithms for band-diagonal matrices can be utilized to minimize the computational time.

3. Modified wave number analysis

The modified wave number analysis is commonly used to determine the resolution property of a numerical scheme. For the B-spline collocation method, the modified wave number for the first and second derivatives, κ' and κ'', can be expressed analytically as (see Kravchenko and Moin [6] for derivations)

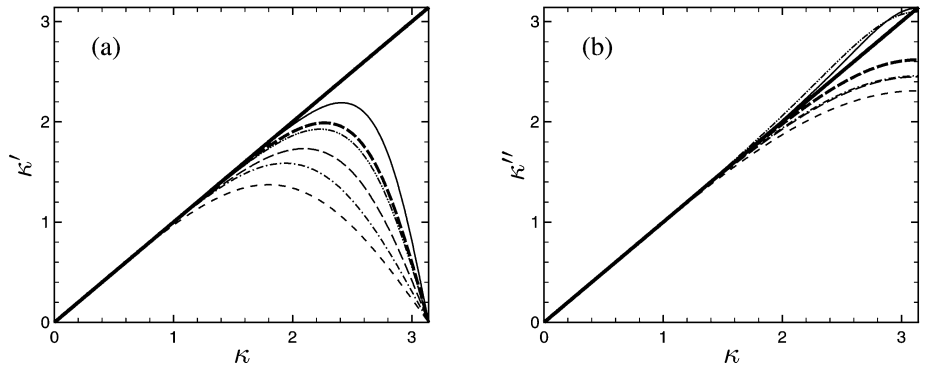

Fig. 2. Modified wave numbers for (a) the first derivative and (b) the second derivative for spectral (▬); FD4 (- - -); FD6 (-·-·-); CD4 (– – –); CD6 (▬ ▬ ▬); BSC4 (-·-·-·-); and BSC6 (——) methods.

Fig. 2. Nombres d'onde modifiés pour (a) la premiére dérivée et (b) la deuxiéme dérivée pour les méthodes spectral (▬); FD4 (- - -); FD6 (-·-·-); CD4 (– – –); CD6 (▬ ▬ ▬); BSC4 (-·-·-·-); et BSC6 (——).

$$\kappa'(\kappa) = \frac{-\sum_{i=1}^{I} 2D_{ij}\sin(i\kappa)}{M_{0j} + \sum_{i=1}^{I} 2M_{ij}\cos(i\kappa)} \quad \text{and} \quad \big(\kappa''(\kappa)\big)^2 = \frac{-\sum_{i=1}^{I} 2V_{ij}(1-\cos(i\kappa))}{M_{0j} + \sum_{i=1}^{I} 2M_{ij}\cos(i\kappa)}$$

where I is the half bandwidth size of the $[M]$, $[D]$ and $[V]$ matrices. The subscript j is chosen such that the mesh point $x_i = 0$ is located at the peak of jth B-spline.

The modified wave numbers of 4th and 6th order B-spline collocation methods (BSC4, BSC6) are compared to those of 4th and 6th order finite difference (FD4, FD6) and compact difference (CD4, CD6) schemes in Fig. 2. The B-spline collocation method is shown to be capable of correctly representing the waves up to a higher wave number than the other schemes of the same order. The unique convergence of κ'' of the B-spline collocation method at higher wave numbers demonstrates its superiority in resolution for high wave number waves. This reduces the number of grid points required in the computation.

4. Acoustic field from a spinning co-rotating vortex pair

To demonstrate the application of the B-spline collocation method, the acoustic field from a spinning co-rotating vortex pair is simulated. As shown in Fig. 3, the vortices whose strengths are $\Gamma = \pi$ are separated at a distance of $2R = 10$ between the cores. They rotate about their mid point with a rotation rate of $\Omega = \frac{\Gamma}{4\pi R^2} = 0.01$ and a rotating Mach number of $M_r = \frac{\Gamma}{4\pi R c_0} = 0.05$ where c_0 is the speed of sound. The profiles of the vortices are modelled using Gaussian vortex which vorticity distribution is given by

$$\omega_z = \frac{\Gamma}{\pi}\exp\big(-r^2\big).$$

The corresponding velocity field can be obtained by solving the streamfunction Poisson equation,

$$\nabla^2\psi = -\omega_z$$

where $\vec{u} = \nabla \times (\psi\hat{k})$, and $\hat{k}$ is the unit vector normal to the plane of rotation.

In the acoustic calculation, Powell's acoustic analogy is used to simulate the production and radiation of the acoustic waves. The governing equation is

$$\frac{1}{c_0^2}\frac{\partial^2 p}{\partial t^2} - \nabla^2 p = \rho_0 \nabla\cdot(\vec{\omega}\times\vec{u}) \tag{3}$$

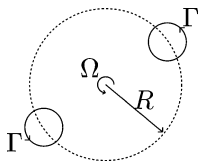

Fig. 3. Schematic diagram of flow configuration.

Fig. 3. Diagramme schématique de la configuration de l'écoulement.

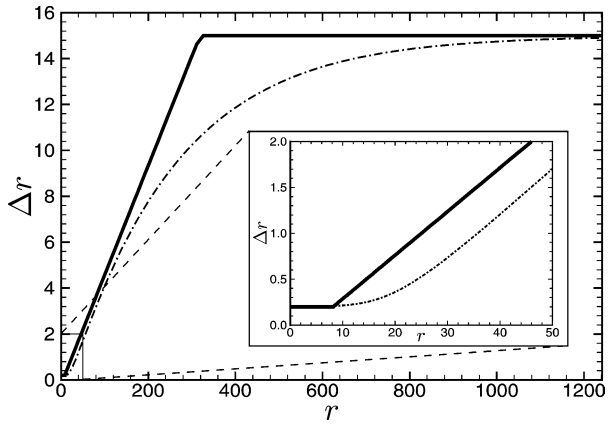

Fig. 4. Radial grid spacings using B-splines (▬); and mapping function (–·–·–).

Fig. 4. Espacement radial du réseau de points en utilisant les courbes B-splines (▬) ; et une fonction de mapping (–·–·–).

where p is the acoustic pressure fluctuation, $\vec{\omega}$ is the vorticity and ρ_0 is the fluid density. The right-hand side of Eq. (3) is called the acoustic source and is computed using the incompressible flow parameters. The acoustic field is simulated using a polar coordinate system. At the computational boundary ($r_{\text{boundary}} = 1241.5$), a radiation boundary condition based on Tam [7] is applied to convect the acoustic waves out of the domain. The spatial derivatives are calculated using the 6th order B-spline collocation method and a Fourier Galerkin method.

The domain discretization uses 192×64 grid points in the radial and azimuthal directions respectively. The radial mesh is non-uniform while the azimuthal mesh is uniform. The radial discretization involves three regions, a uniform fine mesh ($\Delta r_{\text{near}} = 0.2$) in the near field, a uniform coarser mesh ($\Delta r_{\text{far}} = 15$) in the far field and a stretched mesh ($lsf = 0.05$) connecting the two meshes. A plot of grid spacing at different radial position is given in Fig. 4. The discontinuity in the slope at the intersections of the regions, which is a problem when using a mapping function, does not deteriorate the accuracy of the B-spline collocation method. This flexibility allows the grids to be distributed optimally. For a comparison, a continuous hyperbolic tangent mapping function is also plotted in Fig. 4. The mapping function results in 242 grid points, which is 26% more than that using B-splines.

Furthermore, the acoustic field is time marched using a 4th order Runge–Kutta scheme with a time step of $\Delta t = 0.125$. This results in a maximum CFL number of 0.625. The effect of the initial acoustic transient is minimized by employing a ramping function and a numerical filter proposed by S.K. Lele [3].

Fig. 5(a) shows the acoustic field at $t = 3700$ whereby the acoustic field has reached its steady periodic state. The vortices are located close to the center of the domain. They generate a pair of positive and a pair of negatives spikes in the near field as they rotate. This spike pattern denotes a quadrupole source for the acoustic radiation. The radiated acoustic waves have a wavelength of $\lambda = 314$. Its amplitude decays as $r^{-1/2}$ in the far field, which is in agreement with 2D wave propagation theory. The acoustic field can be further validated against the matched asymptotic solution which is given by

$$p(r,\theta,t) = \frac{-\rho_0 \Gamma^4}{64\pi^3 R^4 c_0^2}\left[J_2\left(\frac{2\Omega r}{c_0}\right)\sin(2\theta - 2\Omega t) + Y_2\left(\frac{2\Omega r}{c_0}\right)\cos(2\theta - 2\Omega t)\right] \tag{4}$$

where $J_2(\frac{2\Omega r}{c_0})$ and $Y_2(\frac{2\Omega r}{c_0})$ are second order Bessel functions of the first and second kinds.

Shown in Fig. 5(b) is the radial cut of the acoustic field at $\theta = 0°$. The far field acoustic signal agrees very well with Eq. (4). In the near field however, there are some discrepancies at $r < 20$. This is due to the fact that the analytical solution based on matched asymptotic expansions is derived assuming point vortices where the vorticity

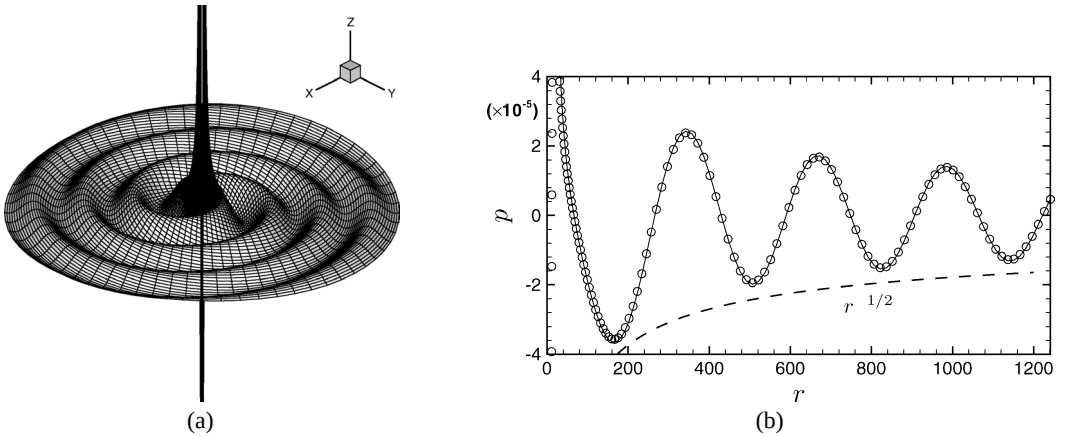

Fig. 5. (a) Acoustic field from the spinning co-rotating vortices at $t = 3700$ and (b) comparison of radial cut of acoustic field at $\theta = 0^\circ$ (∘) to the matched asymptotic solution (——).

Fig. 5. (a) Champ acoustique généré par la rotation de tourbillons co-rotatifs à $t = 3700$ et (b) comparaison du champ acoustique sur une coupe radiale à $\theta = 0^\circ$ (∘) avec la solution asymtotique correspondante (——).

is concentrated at a single point at the vortex core. These discrepancies in the near field were also observed by Slimon, Soteriou and Davis [8].

5. Conclusion

A collocation method based on B-splines as the trial functions is proposed. Its unique arbitrary grid placement capability is shown to be efficient in resolving the flow and acoustic length scales with 26% fewer grid points than that using a hyperbolic mapping function. Moreover, the resolution property of the B-spline collocation method is found to be superior to finite difference and compact difference schemes. Along with its robust formulation, these features make the B-spline collocation method be a suitable method for computational aero-acoustics.

Acknowledgements

This research is funded by Defence Science and Technology Organization, Australia and supported by Commonwealth Scientific and Industrial Research Organization, Australia. The computer resources are supplied by Advanced Research Computing Center at University of Melbourne.

References

[1] C.K.W. Tam, Computational aeroacoustics: issues and methods, AIAA J. 33 (1995) 1788–1796.
[2] C.K.W. Tam, J.C. Webb, Dispersion-relation-preserving finite difference schemes for computational acoustics, J. Comput. Phys. 107 (1993) 262–281.
[3] S.K. Lele, Compact finite difference schemes with spectral-like resolution, J. Comput. Phys. 103 (1992) 16–42.
[4] J.W. Kim, D.J. Lee, Optimized compact finite difference schemes with maximum resolution, AIAA J. 34 (1996) 887–893.
[5] Y. Morinishi, S. Tamano, K. Nakabayashi, A DNS algorithm using B-spline collocation method for compressible turbulent channel flow, Comput. Fluids 32 (2003) 751–776.
[6] A.G. Kravchenko, P. Moin, B-spline methods and zonal grids for numerical simulations of turbulent flow, Ph.D. Thesis, Stanford University, 1998.
[7] C.K.W. Tam, Advances in numerical boundary conditions for computational aeroacoustics, J. Comput. Phys. 6 (1998) 377–402.
[8] S.A. Slimon, M.C. Soteriou, D.W. Davis, Computational aeroacoustics simulations using the expansion about incompressible flow approach, AIAA J. 37 (1999) 409–416.